Anisotropic Electron-Phonon Interaction in the Cuprates

T. P. Devereaux
Department of Physics, University of Waterloo, Ontario, Canada N2L 3GI

T. Cuk and Z.-X. Shen
Department of Physics, Applied Physics, and Stanford Synchrotron Radiation Laboratory, Stanford University, California 94305, USA

N. Nagaosa
CREST, Department of Applied Physics, University of Tokyo, Bunkyo-ku, Tokyo 113-8656, Japan
(Received 19 March 2004; published 10 September 2004)

We explore manifestations of electron-phonon coupling on the electron spectral function for two phonon modes in the cuprates exhibiting strong renormalizations with temperature and doping. Applying simple symmetry considerations and kinematic constraints, we find that the out-of-plane, out-of-phase O buckling mode (B_{1g}) involves small momentum transfers and couples strongly to electronic states near the antinode while the in-plane Cu-O breathing modes involve large momentum transfers and couples strongly to nodal electronic states. Band renormalization effects are found to be strongest in the superconducting state near the antinode, in full agreement with angle-resolved photoemission spectroscopy data.

DOI: 10.1103/PhysRevLett.93.117004 PACS numbers: 74.72.–h, 71.38.–k, 72.10.–d, 79.60.–i

The electron-phonon interaction in metals is generally considered to be isotropic. Recent developments in the cuprates, however, raise important questions about this assumption. The renewed interest stems from the observation of bosonic band renormalization effects in a wide range of p-type materials [1]. This effect is found to be dramatically enhanced below T_c near the $(\pi, 0)$ regions in the Brillouin zone (BZ) [2]. Such a momentum and temperature dependence appears to support the idea that the bosonic renormalizations in p-type materials are due to a coupling of the electrons to the 41 meV spin resonance mode that appears below T_c [3,4].

On the other hand, it has been argued that the bosonic renormalization effect may be reinterpreted as a result of a coupling to the half-breathing in-plane Cu-O bond-stretching phonon for nodal directions [5] and the out-of-plane out-of-phase O buckling B_{1g} phonon for antinodal directions [6]. This reinterpretation has a clear advantage over the spin resonance in that it naturally explains why the band renormalization effect is observed under three circumstances: (1) in materials where no spin mode has been detected, (2) in the normal state, and (3) in the deeply overdoped region where the spin mode is neither expected nor observed. However, this reinterpretation also requires the electron-phonon interaction to be highly anisotropic and its impact on the electrons to be strongly enhanced in the superconducting state. This is something one does not expect *a priori*.

This Letter investigates the anisotropy of the electron-phonon interaction of two known phonons—the half-breathing mode and the B_{1g} buckling mode—formulated within the same framework as that used to explain phonon line shape changes observed via Raman and neutron measurements [4,7–9]. We find the electron-phonon interactions to be very anisotropic as a consequence of the following four properties of the cuprates: (1) the symmetry of the phonon polarizations and electronic orbitals involved leading to highly anisotropic electron-phonon coupling matrix elements $g(k, q)$; (2) the kinematic constraint related to the anisotropy of the electronic band structure and the van Hove singularity (VHS); (3) the d-wave superconducting gap; and (4) the near degeneracy of energy scales of the B_{1g} phonon, the superconducting gap, and the VHS. Taking into account these and thermal effects, we can naturally explain the observed momentum and temperature dependence of the data, leading to unified understanding of band renormalizations.

Our starting point is the tight-binding three-band Hamiltonian modified by B_{1g} buckling vibrations as considered in Ref. [10] and in-plane breathing vibrations as considered in Ref. [11]:

$$\begin{aligned} H = & \sum_{\mathbf{n},\sigma} \epsilon_{\mathrm{Cu}} b^{\dagger}_{\mathbf{n},\sigma} b_{\mathbf{n},\sigma} + \sum_{\mathbf{n},\delta,\sigma} \{\epsilon_{\mathrm{O}} + eE_z u^{\mathrm{O}}_{\delta}(\mathbf{n})\} a^{\dagger}_{\mathbf{n},\delta,\sigma} a_{\mathbf{n},\delta,\sigma} \\ & + \sum_{\mathbf{n},\delta,\sigma} P_{\delta}[t - Q_{\delta} g_{dp} u^{\mathrm{O}}_{\delta}(\mathbf{n})](b^{\dagger}_{\mathbf{n},\sigma} a_{\mathbf{n},\delta,\sigma} + \mathrm{H.c.}) \\ & + t' \sum_{\mathbf{n},\delta,\delta'} P_{\delta,\delta'} (a^{\dagger}_{\mathbf{n},\delta} a_{\mathbf{n},\delta',\sigma} + \mathrm{H.c.}) \end{aligned} \tag{1}$$

with Cu-O hopping amplitude t, O-O amplitude t', and $\epsilon_{d,p}$ denoting the Cu and O site energies, respectively. Here $a_{\alpha=x,y}$, $a^{\dagger}_{\alpha=x,y}$ $(b, b^{\dagger})$ annihilates, creates an electron in the O_{α} (Cu) orbital, respectively. The overlap factors Q_{δ}, P_{δ}, and $P_{\delta,\delta'}$ are given in our notation as $Q_{\pm x} = Q_{\pm y} = \pm 1$, $P_{\pm x} = -P_{\pm y} = \pm 1$, and $P_{\pm x,\pm y} = 1 = -P_{\mp x,\pm y}$. For the half-breathing mode we consider only

couplings $g_{dp} = q_0 t$ (with $1/q_0$ a length scale) arising from modulation of the covalent hopping amplitude t [11,12]. For the B_{1g} mode a coupling to linear order in the atomic displacements arises from a local c-axis oriented crystal field E_z, which breaks the mirror plane symmetry of the Cu-O plane [10].

The symmetry of the p, d wave functions of the Cu-O plane is embedded in the amplitudes ϕ of the tight-binding wave functions forming the antibonding band with energy dispersion $\epsilon(\mathbf{k})$ arising from Eq. (1). Specifically, the transformation is determined by the projected part of the tight-binding wave functions $b_{\mathbf{k},\sigma} = \phi_b(\mathbf{k}) d_{\mathbf{k},\sigma}$ and $a_{\alpha,k,\sigma} = \phi_\alpha(\mathbf{k}) d_{\mathbf{k},\sigma}$,

$$\phi_b(\mathbf{k}) = \frac{1}{N(\mathbf{k})}[\epsilon^2(\mathbf{k}) - t'^2(\mathbf{k})], \tag{2}$$

$$\phi_{x,y}(\mathbf{k}) = \frac{\mp i}{N(\mathbf{k})}[\epsilon(\mathbf{k}) t_{x,y}(\mathbf{k}) - t'(\mathbf{k}) t_{y,x}(\mathbf{k})], \tag{3}$$

with $N^2(\mathbf{k}) = [\epsilon^2(\mathbf{k}) - t'^2(\mathbf{k})]^2 + [\epsilon(\mathbf{k}) t_x(\mathbf{k}) - t'(\mathbf{k}) t_y(\mathbf{k})]^2 + [\epsilon(\mathbf{k}) t_y(\mathbf{k}) - t'(\mathbf{k}) t_x(\mathbf{k})]^2$, $t_\alpha(\mathbf{k}) = 2t \sin(k_\alpha a/2)$, and $t'(\mathbf{k}) = 4t' \sin(k_x a/2) \sin(k_y a/2)$.

The projected wave functions act in conjunction with the phonon eigenvectors to determine the full symmetry of the electron-phonon coupling: $H_{\text{el-ph}} = \frac{1}{\sqrt{N}} \sum_{\mathbf{k},\mathbf{q},\sigma,\mu} g_\mu(\mathbf{k},\mathbf{q}) c^\dagger_{\mathbf{k},\sigma} c_{\mathbf{k}+\mathbf{q},\sigma} [a^\dagger_{\mu,\mathbf{q}} + a_{\mu,-\mathbf{q}}]$. Neglecting the motion of the heavier Cu atoms compared to O in the phonon eigenvectors, the form of the respective couplings can be compactly written as

$$g_{B_{1g}}(\mathbf{k},\mathbf{q}) = eE_z \sqrt{\frac{\hbar}{4M_O M(\mathbf{q}) \Omega_{B_{1g}}}} \{\phi_x(\mathbf{k}) \phi_x(\mathbf{k}') \cos(q_y a/2) - \phi_y(\mathbf{k}) \phi_y(\mathbf{k}') \cos(q_x a/2)\}, \tag{4}$$

$$g_{br}(\mathbf{k},\mathbf{q}) = g_{dp} \sqrt{\frac{\hbar}{2M_O \Omega_{br}}} \sum_{\alpha=x,y} \{\phi_b(\mathbf{k}') \phi_\alpha(\mathbf{k}) \cos(k'_\alpha a/2) - \phi_b(\mathbf{k}) \phi_\alpha(\mathbf{k}') \cos(k_\alpha a/2)\}, \tag{5}$$

with $M(\mathbf{q}) = [\cos^2(q_x a/2) + \cos^2(q_y a/2)]/2$ and $\mathbf{k}' = \mathbf{k} - \mathbf{q}$. A simple consequence of symmetry can be observed at small momentum transfers $\mathbf{q}$ where $g_{B_{1g}}(\mathbf{k}, \mathbf{q} = \mathbf{0}) \sim \cos(k_x a) - \cos(k_y a)$, while $g_{br} \sim \sin(qa)$ for any $\mathbf{k}$. Yet for large momentum transfer $\mathbf{q} = (\pi/a, \pi/a)$, $g_{B_{1g}}$ vanishes for all $\mathbf{k}$ while g_{br} has its maximum for $\mathbf{k}$ located on the nodal points of the Fermi surface. This q dependence has been the focus before in context with a $d_{x^2-y^2}$ pairing mechanism [13,14], but the dependence on fermionic wave vector $\mathbf{k}$ has usually been overlooked. It is exactly this fermionic dependence that we feel is crucially needed to interpret angle-resolved photoemission spectroscopy (ARPES) data.

These features of each coupling constant can be seen in Fig. 1, which plots $|g(\mathbf{k},\mathbf{q})|^2$ as a function of phonon scattered momentum $\mathbf{q}$ connecting initial $\mathbf{k}$ and final

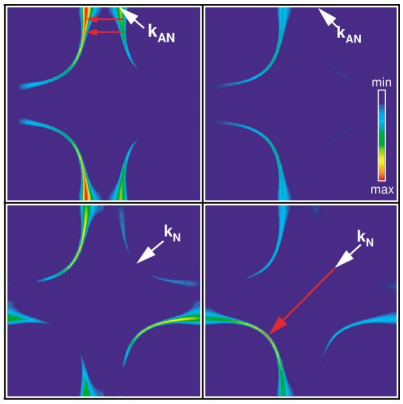

FIG. 1 (color). Plots of the electron-phonon coupling $|g(\mathbf{k},\mathbf{q})|^2$ for initial $\mathbf{k}$ and scattered $\mathbf{k}' = \mathbf{k} - \mathbf{q}$ states on the Fermi surface for the buckling mode (left panels) and breathing mode (right panels) for initial fermion $\mathbf{k}$ at an antinodal (top panels) and a nodal (bottom panels) point on the Fermi surface, as indicated by the arrows. The red or blue color indicates the maximum or minimum of the el-ph coupling vertex in the BZ for each phonon.

$\mathbf{k}' = \mathbf{k} - \mathbf{q}$ fermion states both on the Fermi surface. Here we have adopted a five-parameter fit to the band structure used previously for optimally doped Bi-2212 [3]. For an antinodal initial fermion $\mathbf{k}_{AN}$, the coupling to the B_{1g} phonon is largest for $2\mathbf{k}_F$ scattering to an antinodal final state. The coupling to the breathing mode is much weaker overall, and is especially weak for small $\mathbf{q}$ and mostly connects to fermion final states at larger $\mathbf{q}$. For a nodal fermion initial state $\mathbf{k}_N$, the B_{1g} coupling is suppressed for small $\mathbf{q}$ and has a weak maximum towards antinodal final states, while the breathing mode attains its largest value for scattering to other nodal states, particularly to state $-\mathbf{k}_N$.

In Fig. 2 we show effective couplings $\lambda_{\mathbf{k}}$ (summed over all $\mathbf{q}$) for $\mathbf{k}$ points in the first quadrant of the BZ in the normal state [14]. Here we have used the value of the electric field $eE_z = 1.85$ eV/Å consistent with Raman

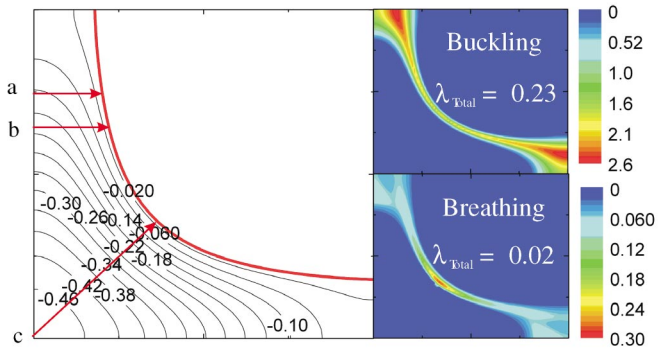

FIG. 2 (color). Plots of the electron-phonon coupling $\lambda_{\mathbf{k}}$ in the first quadrant of the BZ for the buckling mode (right top panel) and the breathing mode (right bottom panel). The color scale is shown on the right for each phonon. The left panel shows energy contours for the band structure used [3].

scattering measurements of the B_{1g} phonon and buckling of the Cu-O plane in YBaCuO, and have taken $q_0 t = 2\sqrt{2} e E_z$ as a representative value for the coupling to the breathing mode. These values lead to net couplings similar to that obtained from local density approximation calculations [14]. As a result of the anisotropy of the coupling constant, large enhancements of the coupling near the antinode for the B_{1g} phonon, and nodal directions for the breathing phonon mode are observed, respectively, which are an order of magnitude larger than the average λ's.

We now turn to the spectral function. The dynamic nature of the coupling is governed by the energy scales of the band structure, phonon frequencies, and superconducting gap energy, and are manifest in features of the Nambu-Eliashberg electron-phonon self-energy [15]: $\hat{\Sigma}(\mathbf{k}, i\omega_m) = i\omega_m[1 - Z(\mathbf{k}, i\omega_m)]\hat{\tau}_0 + \chi(\mathbf{k}, i\omega_m)\hat{\tau}_3 + \Phi(\mathbf{k}, i\omega_m)\hat{\tau}_1$ with

$$\hat{\Sigma}(\mathbf{k}, i\omega_m) = \frac{1}{\beta N} \sum_{\mathbf{p},\mu,m} g_\mu(\mathbf{k}, \mathbf{p} - \mathbf{k}) g_\mu(\mathbf{p}, \mathbf{k} - \mathbf{p}) D^0_\mu(\mathbf{k} - \mathbf{p}, i\omega_m - i\omega_n) \hat{\tau}_3 \hat{G}^0(\mathbf{p}, i\omega_m) \hat{\tau}_3, \quad (6)$$

with $\hat{G}^0(\mathbf{p}, i\omega_m) = \frac{i\omega_m \tau_0 + \epsilon(\mathbf{p})\hat{\tau}_3 + \Delta(\mathbf{p})\hat{\tau}_1}{(i\omega_m)^2 - E^2(\mathbf{p})}$ and $E^2(\mathbf{k}) = \epsilon^2(\mathbf{k}) + \Delta^2(\mathbf{k})$, with $\hat{\tau}_{i=0\cdots3}$ as Pauli matrices. We take $\Delta(\mathbf{k}) = \Delta_0[\cos(k_x a) - \cos(k_y a)]/2$ with $\Delta_0 = 35$ meV. The bare phonon propagators are taken as $D^0_\mu(\mathbf{q}, i\Omega_\nu) = \frac{1}{2}[\frac{1}{i\Omega_\nu - \Omega_\mu} - \frac{1}{i\Omega_\nu + \Omega_\mu}]$. Here we take dispersionless optical phonons $\hbar\Omega_{B_{1g},br} = 36, 70$ meV, respectively.

The spectral function $A(\mathbf{k}, \omega) = -\frac{1}{\pi} \mathrm{Im}\, G_{11}(k, i\omega \rightarrow \omega + i\delta)$ is determined from Eq. (6) with $\hat{G}(k, i\omega_m) = \{\hat{\tau}_0 i\omega_m Z(\mathbf{k}, i\omega_m) - [\epsilon(\mathbf{k}) + \chi(\mathbf{k}, i\omega_m)]\hat{\tau}_3 - \Phi \times (\mathbf{k}, i\omega_m)\hat{\tau}_1\}^{-1}$ and the coupling constants given by Eqs. (4) and (5). Here we consider three different cuts: along the nodal direction ($k_x = k_y$, denoted by c), and two cuts parallel to the BZ face ($k_y = 0.75\pi/a$, b) and ($k_y = 0.64\pi/a$, a) where bilayer effects are not severe [6], as indicated in Fig. 2.

Our results for the three cut directions are shown in Fig. 3 for the normal ($T = 110$ K) and superconducting ($T = 10$ K) states. One can observe only very weak kink features in the normal state, but a much more pronounced kink at 70 meV in the superconducting state is observed for all the cuts, in excellent agreement with the data [6], shown also in Fig. 3. The dramatic temperature dependence stems from a substantial change in the electronic occupation distribution and the opening of the superconducting gap. In the normal state, the phonon self-energy is a Fermi function at 110 K centered at the phonon frequency, which results in a thermal broadening of $4.4k_BT$ or 50 meV, comparable to phonon frequencies. At 10 K in the superconducting state, on the other hand, the phonon self-energy is sharply defined due to the step-function-like Fermi function and a singularity in the superconducting density of states. These factors, together with the experimental difficulty in detecting a weak effect, conspire to leave the false impression that the bosonic mode merges below T_c, as invoked by the spin resonance scenario [3].

In the superconducting state, the data and the theory exhibit a rich variety of signatures in the electron-phonon coupling: cut a exhibits the strongest signatures of coupling, showing an Einstein-like breakup into a band that follows the phonon dispersion, and one that follows the electronic one; in cut b, a weaker signature of coupling manifests itself in an s-like renormalization of the bare band that traces the real part of the phonon self-energy; and in cut c, where the coupling to the B_{1g} phonon is weakest, the electron-phonon coupling manifests itself as a change in the velocity of the band. The agreement is very good, even for the large change in the electron-phonon coupling seen between cuts a and b, separated by only 1/10th of the BZ.

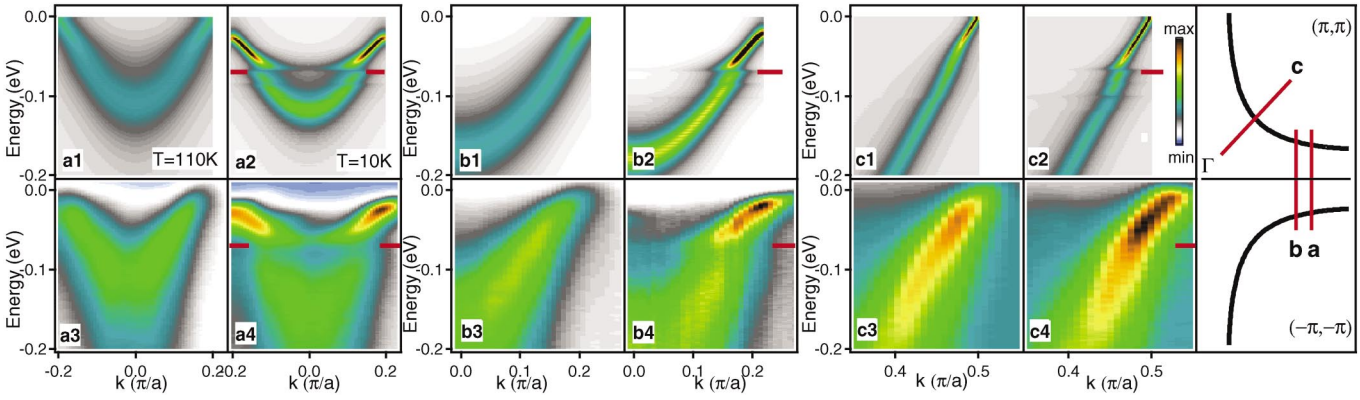

FIG. 3 (color). Image plots of the calculated spectral functions in the normal (a1,b1,c1) and superconducting (a2,b2,c2) states compared to the spectral functions in the normal (a3,b3,c3) and superconducting (a4,b4,c4) states measured in $Bi_2Sr_2Ca_{0.92}Y_{0.08}Cu_2O_{8+\delta}$ (Bi-2212) [6] for momentum cuts a, b, c shown in the rightmost panel and in Fig. 2. The same color scale is used for the normal or superconducting pairs within each cut, but the scaling for the data and the calculation are separate. The red markers indicate 70 meV in the superconducting state.

We now discuss the reason for the strong anisotropy as a result of a concurrence of symmetries, band structure, d-wave energy gap, and energy scales in the electron-phonon problem. In the normal state, weak kinks are observed at both phonon frequencies, but more pronounced at 70 meV for cut c and at 36 meV for cut a, as expected from the anisotropic couplings shown in Fig. 1. However, this is also a consequence of the energy scales of the phonon modes and the bottom of the electronic band along the cut direction as shown in Fig. 2. Further towards the antinode, another interesting effect occurs. As one considers cuts closer to the BZ axis, the bottom of the band along the cut rises in energy and the breathing phonon mode lies below the bottom of the band for ($k_x = 0, k_y > 0.82\pi/a$), and so the kink feature for this mode disappears. This is the usual effect of a Fano redistribution of spectral weight when a discrete excitation lies either within or outside the band continuum [16]. This thus can be used to open "windows" to examine the coupling of electrons to discrete modes in general. Taken together, this naturally explains why the normal state nodal kink is near 70 meV [5] while the antinodal kink is near 40 meV [2,6].

In the superconducting state the bare band renormalizes downward in energy due to the opening of the gap and gives the strongest effect for the antinodal region where the gap is of the order of the saddle point energy. The B_{1g} coupling becomes dramatically enhanced by the opening of the gap at a frequency close to the frequency of the phonon itself, and leads to the dramatic renormalization of the phonon observed in Raman and neutron measurements [7]. Yet the breathing coupling does not vary dramatically as the large gap region is not weighted as heavily by the coupling constant. As a consequence, the B_{1g} mode dominates and clear kinks in the data are revealed at around 70 meV—the B_{1g} energy plus the gap. Indeed, a much weaker kink at 105 meV from the breathing phonon shows at higher energies for the nodal cut, but this kink becomes weaker away from nodal directions as the coupling and the band bottom along the cut moves below the phonon frequency so that the "energy window" closes.

Our work is formulated in the context of band structure and one phonon process. Figure 3 indicates that such an approach catches the key features of the band renormalization effects due to optical phonons in the 35–70 meV range, something unexpected *a priori* given the strong correlation effects in these materials. Additional broadening in the data of Fig. 3 is likely a manifestation of the Coulomb correlation over a broad energy range. A next step is to incorporate the correlation effect, vertex correction, and possible nonlinear phonon effects, especially as we push towards underdoped regime. These are challenges ahead. On the other hand, the current approach allows us to study the doping trend in the overdoped regime.

In summary, contrary to the usual opinion of the role of anisotropy in electron-phonon coupling, the interplay of specific coupling mechanisms of electrons to the buckling and breathing phonons give a natural interpretation to the bosonic renormalization effects seen in ARPES in both the normal and superconducting states, and provides a framework to understand renormalizations as a function of doping.

ARPES data were collected at SSRL, which is operated by DOE under Contract No. DE-AC03-76SF00515. T. P. D. acknowledges support from NSERC, PREA, and the A. von Humboldt Foundation. The Stanford work is also supported by NSF Grant No. DMR-0304981 and ONR Grant No. N00014-01-1-0048.

[1] A. Damscelli, Z. Hussain, and Z.-X. Shen, Rev. Mod. Phys. **75**, 473 (2003), and references therein.
[2] A. Gromko *et al.*, Phys. Rev. B **68**, 174520 (2003); T. Sato *et al.*, Phys. Rev. Lett. **91**, 157003 (2003); T. K. Kim *et al.*, Phys. Rev. Lett. **91**, 167002 (2003).
[3] M. R. Norman *et al.*, Phys. Rev. B **64**, 184508 (2001); M. Eschrig and M. R. Norman, Phys. Rev. Lett. **85**, 3261 (2000); Phys. Rev. B **67**, 144503 (2003); A. V. Chubukov and M. R. Norman, cond-mat/0402304.
[4] H.-Y. Kee *et al.*, Phys. Rev. Lett. **88**, 257002 (2002); Ar. Abanov *et al.*, Phys. Rev. Lett. **89**, 177002 (2002).
[5] A. Lanzara *et al.*, Nature (London) **412**, 510 (2001); Z.-X. Shen *et al.*, Philos. Mag. B **82**, 1349 (2002); X. J. Zhou *et al.*, Nature (London) **423**, 398 (2003).
[6] T. Cuk *et al.* (to be published).
[7] B. Friedl *et al.*, Phys. Rev. Lett. **65**, 915 (1990); N. Pyka *et al.*, Phys. Rev. Lett. **70**, 1457 (1993); D. Reznik *et al.*, Phys. Rev. Lett. **75**, 2396 (1995).
[8] S. L. Chaplot *et al.*, Phys. Rev. B **52**, 7230 (1995); R. J. McQueeney *et al.*, Phys. Rev. Lett. **82**, 628 (1999); **87**, 077001 (2001); J.-H. Chung *et al.*, Phys. Rev. B **67**, 014517 (2003); S. Sugai *et al.*, Phys. Rev. B **68**, 184504 (2003).
[9] M. Opel *et al.*, Phys. Rev. B **60**, 9836 (1999).
[10] T. P. Devereaux, A. Virosztek, and A. Zawadowski, Phys. Rev. B **59**, 14 618 (1999); **51**, 505 (1995).
[11] S. Barišić, Phys. Rev. B **5**, 932 (1972).
[12] The coupling g_d arising from modulation of Cu site energies leads to a coupling that depends only on momentum transfers and not on fermion momentum [11].
[13] D. J. Scalapino, J. Phys. Chem. Solids **56**, 1669 (1995); A. Nazarenko and E. Dagotto, Phys. Rev. B **53**, 2987 (1996); T. S. Nunner, J. Schmalian, and K. H. Bennemann, Phys. Rev. B **59**, 8859 (1999).
[14] O. Jepsen *et al.*, J. Phys. Chem. Solids **59**, 1718 (1998).
[15] A. W. Sandvik *et al.*, Phys. Rev. B **69**, 094523 (2004).
[16] U. Fano, Phys. Rev. **124**, 1866 (1961).